Journal of
Synchrotron Radiation
ISSN 0909-0495

Received 3 September 2008
Accepted 23 October 2008

A combined microRaman and microdiffraction set-up at the European Synchrotron Radiation Facility ID13 beamline

Richard J. Davies,* Manfred Burghammer and Christian Riekel

European Synchrotron Radiation Facility, 6 rue Jules Horowitz, BP 220, 38043 Grenoble Cedex, France. E-mail: rdavies@esrf.fr

This article describes the current status of the microRaman set-up at the ID13 beamline of the European Synchrotron Radiation Facility. This offers an *in situ* on-axis microprobe which has a common focal position to the X-ray microbeam and can collect spectral data simultaneously. It can also be used in an offline sample characterization role, both before and after beamline experiments. To demonstrate the application of microRaman spectroscopy within a beamline environment, a number of examples are given.

Keywords: microfocus; X-ray diffraction; Raman spectroscopy.

1. Introduction

Raman spectroscopy and X-ray diffraction are techniques that provide complementary information. Wide-angle X-ray scattering (WAXS) provides information concerning crystallographic structure and texture whilst small-angle X-ray scattering (SAXS) gives access to electron density variations corresponding to large-scale structures. By contrast, the information provided by Raman spectroscopy can be associated with changes in the vibrational and rotational energies of individual molecular bonds during excitation. Not only do the two techniques therefore provide information relating to complementary length scales, they also exhibit different phase sensitivities.

Both X-ray diffraction and Raman spectroscopy can be performed with microbeams. This allows local structure to be probed in heterogeneous samples and enables data collection from smaller volumes (owing to the higher flux density). MicroRaman spectroscopy (μRaman) is available as a standard laboratory tool using high-brilliance laser beam excitation. By contrast, X-ray microdiffraction (μXRD) has only become available as a routine tool with the development of high-brilliance undulators at third-generation synchrotron radiation sources, such as the European Synchrotron Radiation Facility (ESRF).

The combination of X-ray diffraction and Raman spectroscopy has already been reported for macroscopic beams (Bras & Ryan, 1996; Bryant *et al.*, 1998; Ran *et al.*, 2003; McGeehan *et al.*, 2007; Boccaleri *et al.*, 2007). The *in situ* coupling of μRaman and μXRD, however, has only recently been realised (Davies *et al.*, 2005). For their combination to be meaningful, the two techniques must share a common focal position and beam spot size on the sample, whilst data collection should be carried out simultaneously. This requires the development of dedicated instrumentation that not only has this capability, but allows data collection from the two instruments without any interference with one another's operation.

The difficulties of combining μRaman spectroscopy and μXRD together need to be balanced against the benefits that their combination brings. The greatest benefit comes from the assurance of a temporal and spatial correlation between the two instruments. With microfocus probes, many materials appear highly heterogeneous. This can make it extremely challenging to locate precisely the same region on a sample in two separate experiments, especially when variations may not be visible optically. Similarly, there can be considerable local variability during dynamic studies when a microfocus technique is used. For example, although the deformation of a bulk material may be reproducible macroscopically, on the microscale there can be local stress concentrations. Unless both microprobes are monitoring precisely the same region on the sample, and over the same time frame, it is practically impossible to duplicate local behaviour in sequential experiments. Thus, there are considerable advantages of combining μRaman spectroscopy and μXRD together *in situ*. Indeed, owing to these considerations, many materials cannot be studied in *ex situ* experiments using the two instruments independently.

ID13 has recently installed and commissioned a unique custom-built μRaman spectrometer for simultaneous Raman and μXRD data collection (Davies *et al.*, 2003, 2005). The combination of the two techniques guarantees a common focal position and simultaneous data collection between the two instruments. In doing so it eliminates many of the problems associated with performing experiments sequentially. This article describes the current ID13 beamline and μRaman set-

up in detail and includes some examples of typical beamline applications. These correspond to both *in situ* and offline laboratory use.

2. Overview of the ID13 beamline

The ID13 beamline specializes in the delivery of micro- and nano-focused X-ray beams for SAXS/WAXS applications (Riekel & Davies, 2005). Access to the beamline is granted biannually, either by the submission of peer-reviewed proposals or as proprietary research. The majority of experiments fall within the field of soft condensed matter, such as investigations into polymers and biomaterials (Riekel & Davies, 2005; Riekel, 2000). The flexibility of the beamline also allows many other subjects to be studied, however, such as protein crystallography, materials science and environmental research.

The primary radiation source at ID13 is an 18 mm in-vacuum undulator with an optimum brilliance for its first harmonics at about 13 keV (Chavanne *et al.*, 2000). A 46 mm undulator is also available for special applications which require a large tuning range. The beamline itself is linear, with an optics hutch housing a liquid-nitrogen-cooled channel-cut Si(111) monochromator and three experimental hutches. The first two experimental hutches (EH1 and EH2) are used for microfocus applications. A dedicated microdiffraction set-up in EH2 offers beam sizes of around 1 µm, coupled with a high degree of modularity and flexibility. EH1, meanwhile, is currently being refurbished for experiments requiring extended beam time. The third hutch, EH3, is located outside of the experimental hall. This is optimized for beam sizes $\leq$200 nm requiring ultra-stable operation. A beam size of 50 nm has recently been demonstrated (Schroer *et al.*, 2005). A schematic floor plan of ID13 is shown in Fig. 1.

In terms of focusing optics, a number of different systems are in routine use at ID13. These include compound refractive lenses (Lengeler *et al.*, 2001), Kirkpatrick–Baez (KB) mirrors (Hignette *et al.*, 2003) and crossed linear Fresnel optics (Nöhammer *et al.*, 2005). The range of optical systems allows the beam's characteristics to be tailored to individual experimental requirements, whether it is for WAXS or SAXS applications. For data collection, either a MAR CCD or FReLoN detector can be used, both of which have a 2K $\times$ 2K pixel array and 16-bit readout. The MAR CCD has a 165 mm-diameter active area and a readout time of several seconds. For faster data collection, the FReLoN detector offers a 10 Hz readout frequency, with an 80 mm-diameter active area

The high modularity of ID13 makes the beamline suitable for specialist set-ups, such as *in situ* heating (Martel *et al.*, 2007), chemical modification (Schoeck *et al.*, 2007), deformation (Davies *et al.*, 2001) and/or humidity (Glisovic *et al.*, 2008). Microfluidic environments (Martel *et al.*, 2008) and optical tweezers (Cojoc *et al.*, 2007) are also feasible.

3. The ID13 Raman system

The ID13 Raman system was designed and constructed in collaboration with Renishaw plc. The original design objective was to develop a system which could provide the performance of a typical laboratory-based µRaman instrument, whilst being compatible with (and not interfering with) standard beamline operations. In terms of performance the laser spot size would need to match the dimensions of the X-ray beam and be delivered to the same point on the sample simultaneously. Data collection times would also need to be similar between the two instruments. In terms of integration, it is important for the system to be compatible with the position of standard beamline elements. For example, it should still allow X-ray aperture placement upstream of the specimen whilst not shadowing the detector on the downstream side. Finally, owing to the beamline's scientific programme, the system would need to be fully compatible with other *in situ* techniques, such as stretching cells, and must occupy as little of the sample environment as possible.

The resulting design meets all of these criteria and consists of two separate elements. A laboratory-based spectrometer and microscope allows *ex situ* sample characterization whilst a remote probe is provided for *in situ* use. Both systems use the same excitation source, a 785 nm near-IR Toptica diode laser rated at 500 mW. This wavelength was chosen as it minimizes the fluorescence background for many samples. The laser is installed in a parallel configuration to the spectrometer, and in-line with a fibre optic coupling. This arrangement allows laser delivery to either the microscope or remote probe, as necessary. Diversion of the laser is carried out by the insertion of a beam-steering mirror. Further details of the laboratory system and remote probe will now be given.

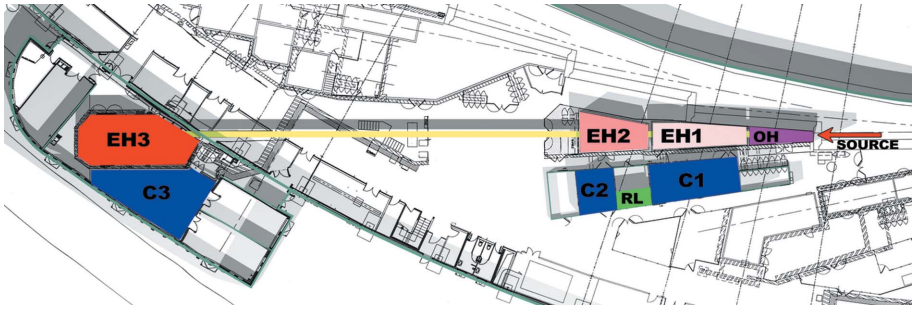

Figure 1
ID13 beamline overview showing the positions of the optics and experimental hutches (OH and EH1-3, respectively), control cabins (C1–C3) and the Raman laboratory (RL).

3.1. Laboratory microRaman system

The ID13 Raman spectrometer is a research-grade InVia system, directly coupled to a Leica microscope. The spectrometer is equipped with a pinhole aperture and beam expander, holographic Rayleigh rejection filters, fully motorized slits and a Peltier-cooled

CCD. This configuration supports both confocal and standard operation modes. A 1200 lines mm^{-1} grating provides a spectral range of approximately 600 cm^{-1} for single-shot (static) acquisitions. Extended scans covering larger ranges are also possible using Renishaw's Synchroscan acquisition mode (or standard spectra stitching techniques).

The microscope is installed within a dedicated enclosure to allow safe operation and reduce spectral artefacts from external sources such as overhead lighting. It is fitted with a selection of objectives (from 5× to 100×), including a long-working-distance objective for studying inaccessible sample environments (such as microfluidic cells). These provide focal spot sizes of between 1.1 µm and 8 µm (corresponding to Airy disc diameters). The microscope stage is fully motorized along all three translation axes (*x*/*y*/*z*) *via* both joystick and software control. This enables lateral and depth mapping experiments to be carried out routinely.

3.2. *In situ* remote probe

The ID13 remote Raman microprobe unit is connected to the spectrometer using two 96 m-long fibre optic cables. A single-mode fibre is used for laser delivery. This maximizes throughput whilst ensuring optimal beam characteristics for subsequent focusing. Meanwhile, a multi-mode fibre is used to return the backscattered light to the spectrometer. A selection of motorized neutral density filters are positioned between the laser source and fibre optic coupling. By attenuating the beam it is possible to adjust laser power at the sample position, reducing the risk of sample damage.

Precise details of the optical system used within the probe remain proprietary. It is based, however, upon a pierced parabolic mirror system which focuses the laser beam to a point situated approximately 0.5 mm from the protective metal plate on the probe head. This arrangement results in a fixed beam spot size of 1.1 µm at the focal position (Davies *et al.*, 2005). The addition of a motorized beam splitter and integrated camera allows the laser spot on the sample to be monitored. Meanwhile, white LED illumination can be used for general sample visualization and to select regions of interest within the field of view. The Raman microprobe unit is shown annotated in Fig. 2. Optical images obtained from the CCD within the probe head are shown in Fig. 3. These represent the system's *in situ* visualization capabilities. The left-hand image shows the attenuated laser spot focused onto a sample whilst the right-hand image shows a single fibre viewed under white-light illumination.

In terms of quantifying the system's overall efficiency, it is difficult to separate the different sources of signal loss from within the instrument. This includes components from the laser source, coupling, optical fibres, focusing optics, filters, grating and CCD. It is therefore more convenient to express overall efficiency (when using the probe) relative to standard microscope operation. The intensity of the 520 cm^{-1} Si Raman band can be used for this purpose, with the microscope operated using a 50× objective (NA = 0.75). This corresponds to a similar spot size on the sample (approximately 1.3 µm using a 785 nm excitation source). Using this comparison, spectral data collected using the remote probe are approximately 10% of the intensity obtained under standard microscope operation. The greatest losses occur between the laser source and optics enclosure ($\geq$50%).

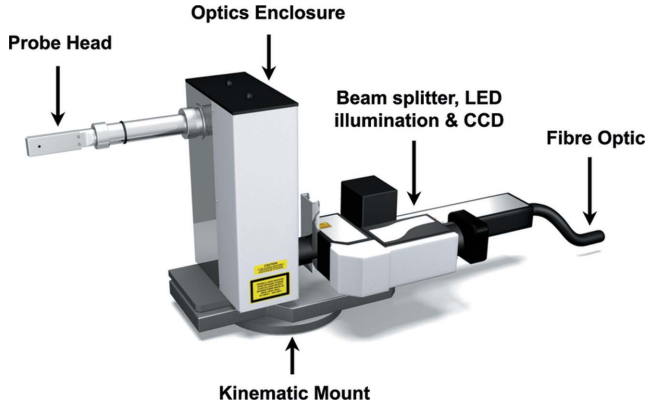

Figure 2
Annotated diagram of the remote Raman microprobe showing the position of major components.

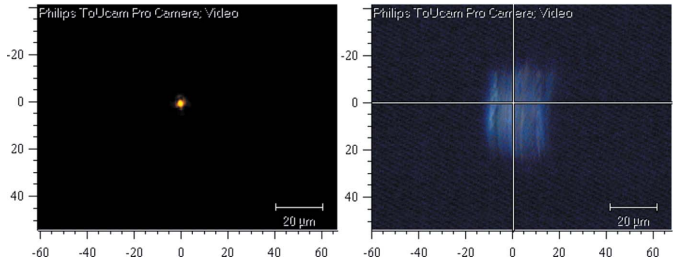

Figure 3
Optical images from the remote probe CCD representing visualization of the attenuated laser spot on the sample (left) and a single fibre observed under white-light illumination (right).

3.3. Beamline integration

The spectrometer and microscope of the ID13 µRaman system are housed within a dedicated laboratory, between the EH1 and EH2 control cabins (see Fig. 1). This temperature-controlled windowless room allows offline operation without interrupting standard beamline operations. The remote Raman microprobe, meanwhile, is currently installed at the microfocus endstation, EH2. This is largely because, although the probe is compatible with a range of different ID13 optics, the crossed-KB mirrors in EH2 can deliver a similar X-ray beam spot size (Riekel & Davies, 2005). It is important to point out, however, that the probe is not permanently tied to this particular experimental hutch. The 96 m length of the fibre optic is designed to allow relocation to any of the ID13 experimental hutches, if required.

The µRaman probe head sits upstream of the X-ray focal position, with the incident laser light being focused downstream onto the sample along the same axis. The Raman scattering is then collected in a backscattering geometry, eliminating the need for further collection elements within the

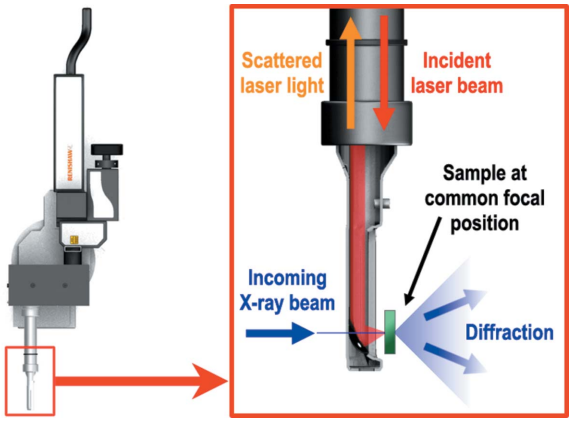

Figure 4
Top-down view of the Raman microprobe with expanded schematic representing simultaneous on-axis data collection geometry for X-ray diffraction and Raman spectra.

sample environment. This arrangement ensures that the probe head will not block any X-ray scattering coming from the sample. Meanwhile it does not interfere with X-ray beam delivery as the hole in the parabolic mirror allows the X-ray beam to pass directly through. The common focal position is therefore made possible by exploiting a difference in divergence between the two beams. Fig. 4 shows a schematic diagram of this simultaneous on-axis data collection.

The remote probe is installed within the ID13 sample environment on a kinematic mount. This ensures repeatable placement of the probe, allowing it to be uninstalled when not in use and reinstalled relatively rapidly. The mount is attached to a fully motorized base ($x/y/z$), for aligning the probe to the X-ray beam position. Such alignment can be achieved by visualizing (on the CCD camera within the probe) a calibration object placed at the X-ray beam focus. This ensures that the focal positions of both instruments coincide.

To achieve simultaneous data collection, the spectrometer and beamline control software are connected by a passive triggering system. During *in situ* experiments, Raman acquisitions can be triggered using a rising-edge pulse from the beamline OPIOM card. This duplicates the signal used to open the beamline fast shutter, controlling X-ray dose. This operation mode enables the simultaneous data collection of X-ray and Raman data. An output level from the spectrometer to the OPIOM card allows the beamline control software to monitor the status of the spectrometer. This ensures no further action is taken, such as moving motors, until both X-ray and Raman data collection has been completed. In this way the two instruments can use different exposure times (if required).

The use of a remotely coupled laser within a beamline environment has certain safety implications. The system therefore incorporates a remote launch box within the experimental hutch which can be inhibited by a key. This secures a shutter in front of the fibre optic coupling when the remote probe is not in use. The launch box also provides a hard-wired remote user interface (UI) connection to the spectrometer control computer within the Raman laboratory. This allows the spectrometer to be controlled remotely from within the experimental hutch if required (*e.g.* for alignment purposes). A second UI extension can be placed within the experimental control cabin. This can be used to configure and monitor Raman data collection during *in situ* use.

3.4. System limitations

The ID13 μRaman system is not without its technical limitations. It is important to point out, however, that many of these extend to microfocus Raman spectroscopy in general. For example, care must be taken not to damage sensitive samples through the use of excessive laser power. Whilst reducing beam brilliance and using much longer exposure times can solve this problem, this solution may not be practical if Raman acquisition times become significantly longer than X-ray exposures. For this reason, *in situ* Raman data collection is more appropriate for samples with comparatively strong Raman scattering, especially in scanning studies over large areas. Of course, this does not preclude the study of weak Raman scatterers *in situ*, but in these cases it should probably be limited to data collection strategies involving single points of interest.

The ID13 μRaman probe head has been designed with laser spot size and collection efficiency as priorities. This necessitates a short working distance between the probe head casing and sample (approximately 0.5 mm). As a result, sample environments where access is limited (such as bulky *in situ* devices) cannot be used. It also prohibits local conditions that would damage or distort the pierced parabolic mirror, such as cryo-cooling and heating. Developments in focusing optics may allow microfocusing with longer working distances in the future. Alternatively, the existing system could be upgraded to include an intermediate option having a longer working distance at the expense of beam spot size and collection efficiency.

There are a number of limitations of the existing system that could be easily overcome by system upgrades. For example, although the current spectrometer has no polarization filters, they could be installed if required. In terms of excitation source, the *in situ* system is currently limited to a single excitation wavelength. Whilst mounting additional lasers is technically feasible, each laser would require a dedicated fibre optic and *in situ* probe.

4. Applications and examples

Two primary applications are foreseen for the ID13 μRaman system. These correspond to general offline sample characterization and *in situ* use. In order to illustrate these different applications, both will now be discussed in greater detail. This also provides an opportunity to demonstrate the system's capabilities through a number of examples.

4.1. General offline sample characterization

A key use of the ID13 μRaman system is for offline sample characterisation. This includes both the characterization of general samples as well as characterizing samples intended for X-ray experiments. This latter application allows visiting user groups to exploit the complementary nature of μXRD and μRaman spectroscopy without performing dedicated combinatorial experiments. It also provides a way to identify regions of interest for later study with X-rays on the beamline. For example, local heterogeneities of a few micrometers can be difficult to observe optically. Not only can spectral differences help isolate features over these length scales, they can also identify materials which appear optically indistinguishable but are chemically and/or structurally different. Conversely, μRaman spectroscopy also has applications for characterizing samples that have already been studied by μXRD. This could be in order to interpret the observed diffraction patterns, or for investigating the extent of radiation damage.

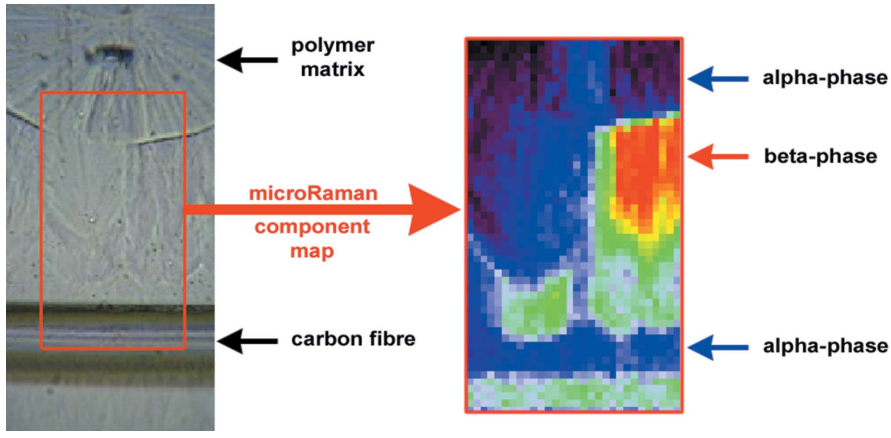

Figure 5
Optical micrograph of a composite material containing a transcrystalline layer around a single carbon fibre (left) and a two-dimensional component map of the phase distribution over the same region determined using offline microRaman spectroscopy (right).

The advantages of operating a Raman spectrometer within a beamline environment for sample characterization are clear. Perhaps less obvious, however, are the indirect benefits that use of the instrument will also bring. For example, by identifying regions (or samples) of interest before (and during) beamline experiments, less beam time will be required performing low-resolution characterization scans with X-rays. This will help ensure that beam time is used as effectively as possible.

To demonstrate the use of μRaman spectroscopy as a general sample characterization tool, Fig. 5 shows a two-dimensional component map of the transcrystalline layer within a fibre reinforced composite (FRC) material. These data were collected offline using the μRaman instrument, with an optical image of the mapped region also shown. The matrix is isotactic polypropylene (PP), surrounding a single carbon fibre as the reinforcing element. In this case the component map corresponds to a linear superposition of component spectra which best represent the different phases of PP. Thus, blue regions in Fig. 5 match the spectral characteristics of α-phase PP, whilst red regions match those of β-phase PP. The resulting phase map reveals how local variations can be resolved within the vicinity of the transcrystalline layer. This corresponds to a layer of β-phase PP near to the carbon fibre, whilst the bulk material and polymer directly adjacent to the fibre remain in the α modification. Such variations have been reported previously for FRC specimens having a PP matrix material (Torre *et al.*, 2006). The example in Fig. 5 demonstrates how regions which appear optically similar can be resolved in terms of different phases using μRaman spectroscopy. As mentioned previously, this could be exploited for locating regions of interest prior to μXRD experiments.

Another example of offline μRaman use is shown in Fig. 6. This corresponds to a map of integrated Raman band intensity covering a region of a polymer film that has been previously used as part of a scanning μXRD experiment on the ID13 beamline. The example demonstrates the use of μRaman spectroscopy for investigating local radiation damage. This type of damage is particularly common during experiments conducted on soft condensed matter samples. The use of a μRaman system allows regions of radiation damage to be spatially resolved offline. In this case the X-ray mesh scan region is clearly visible as a square of lower Raman band

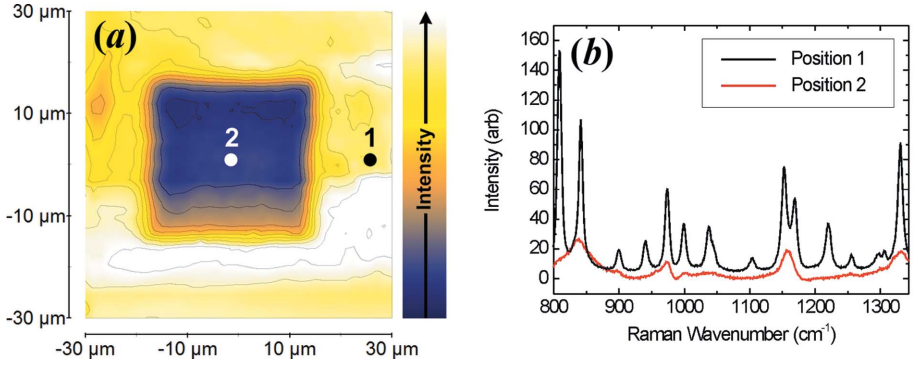

Figure 6
(*a*) Map of integrated Raman band intensity over a polymer film which has previously been used in a scanning microdiffraction experiment. (*b*) Individual spectra from regions (1) outside and (2) inside the irradiated zone. Spectral differences reflect X-ray-induced radiation damage.

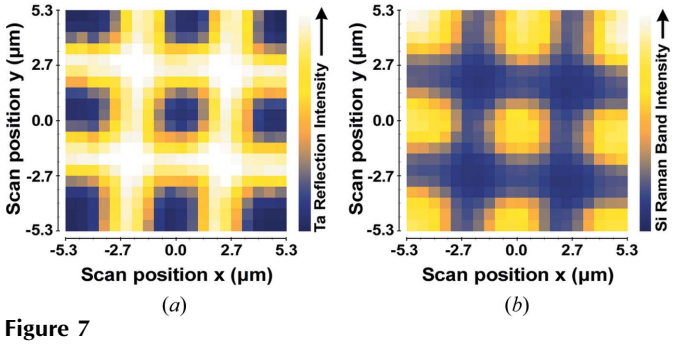

Figure 7
Complementary plots showing the spatial distribution of (*a*) Ta and (*b*) Si determined by combined X-ray microdiffraction and microRaman spectroscopy. Ta distribution is shown by the intensity of the 002 β-phase reflection from X-ray diffraction data. Si distribution is shown from the 520 cm^{-1} Raman band intensity.

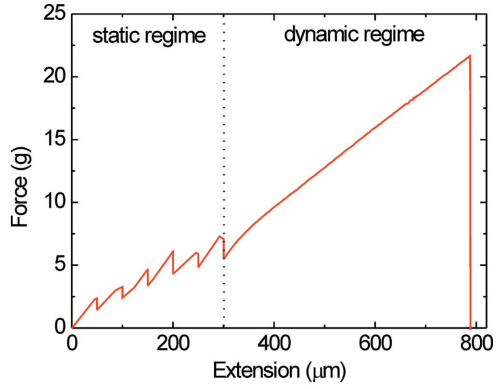

Figure 8
Force–extension plot obtained during the *in situ* deformation of a single HDPE fibre.

intensity at the centre of the image. This represents a scan of 20 × 20 μm using a step size of 2 μm along both axes.

4.2. *In situ* use

Whilst offline characterization is likely to remain the most common use of the ID13 μRaman system, its most important application is undoubtedly *in situ* use. This allows the simultaneous collection of μRaman and μXRD data, from a common focal position on the specimen. As a tool for simultaneous data collection, many different types of experiment can be imagined. In scanning studies the two techniques allow imaging in terms of both X-ray and Raman scattering variations. As mentioned previously, this can provide quite different information about the sample, which is often complementary in nature. An example of this is shown in Fig. 7. In this case the two techniques are able to provide complementary phase information from a two-dimensional raster scan. The laboratory-fabricated sample consists of Ta structures (2 μm width) deposited on a Si membrane (Nöhammer, 2004). The Ta component gives rise to a 002 β-phase reflection whilst the Si component gives a strong Raman band at 520 cm^{-1} (Davies *et al.*, 2005). Using both data sets together, the spatial distribution of each element can be mapped independently. The appearance of the resulting images in Fig. 7 demonstrates a common sampling region between the two techniques. A similar experiment using smaller structures has allowed the laser beam spot size to be determined from modelling (Davies *et al.*, 2005).

Dynamic experiments benefit from the temporal and spatial correlations guaranteed by *in situ* approaches. To demonstrate this, Figs. 8, 9 and 10 show simultaneous μRaman and μXRD during a dynamic experiment performed *in situ*. This corresponds to the deformation of a single high-density polyethylene (HDPE) fibre. Fig. 8 shows the force–extension plot obtained during deformation. This can be divided into static and dynamic deformation regimes. Fig. 9 shows a Raman spectrum and HDPE diffraction pattern collected simulta-

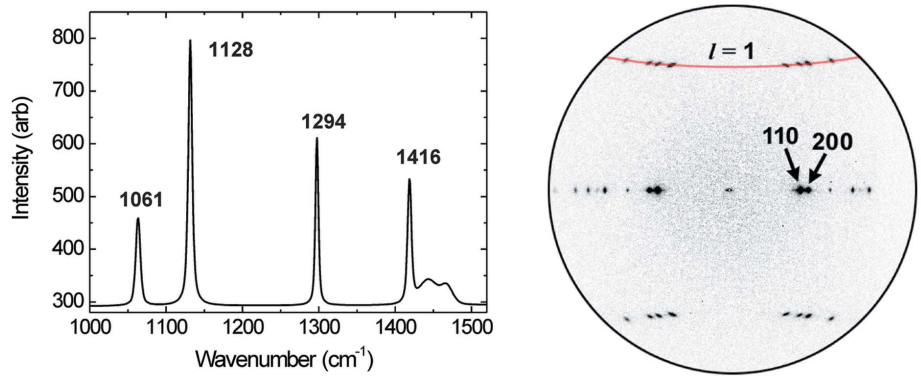

Figure 9
Typical diffraction pattern and Raman spectrum obtained simultaneously *in situ*. Data correspond to an exposure time of 5 s for both instruments.

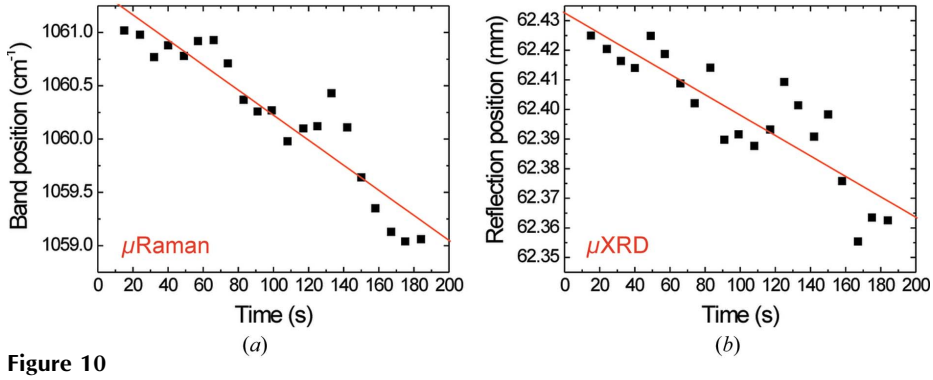

Figure 10
(*a*) Raman band shifts and (*b*) changes in reflection position calculated from Raman spectra and diffraction data collected simultaneously during the *in situ* deformation of a single HDPE fibre.

neously using an exposure time of 5 s. Figs. 10(*a*) and 10(*b*) show Raman band shifts and variations in reflection positions obtained during *in situ* deformation under the dynamic regime. Raman band shifts (Fig. 10*a*) have been determined from the position of the 1061 cm^{-1} Raman band shown in Fig. 9(*a*). This particular band is associated with asymmetric C—C stretching (Rodriguez-Cabello *et al.*, 1998; Lu *et al.*, 1998). Its change in position with applied macroscopic strain demonstrates a distortion of this particular bond owing to stretching of the molecular chain. Changes in reflection position (Fig. 10*b*), meanwhile, have been calculated from the off-axis meridional reflections on the first layer line (Fig. 9*b*). They correspond to distortions of the HDPE crystal lattice along the fibre axis direction (c^*). This demonstrates the stretching of crystalline domains within the fibre.

This example reveals how combined μRaman and μXRD can provide complementary information during dynamic studies. In this case it allows macroscopic deformation to be traced through the different hierarchical structural levels of a material, from the bulk fibre right down to the stretching of individual parts of the HDPE molecule. Such information can then be used to develop models describing deformation behaviour (Davies *et al.*, 2003).

For *in situ* deformation using microbeams, temporal and spatial correlation between data sets is a necessity. Other applications can be envisaged, however, that would also benefit from an *in situ* approach but do not require simultaneous data collection. For example, many samples, and biological systems in particular, are prone to radiation damage during X-ray experiments. By using the *in situ* μRaman system as an alignment tool, a specific region of interest on a sample could be placed at the X-ray beam's position without the need for alignment scans using X-rays. Thus, X-ray-induced radiation damage before data collection could be avoided. An *in situ* system also provides a convenient way of investigating the influence of data collection on the sample. For Raman spectroscopy this allows the online assessment of radiation damage owing to X-ray exposure. Not only can this provide information on the mechanism by which radiation damage occurs, it also gives some idea of its spatial extent (Davies *et al.*, 2008). For X-ray diffraction meanwhile, this allows the online assessment of sample heating at the position of the laser focus. Local heating could be assessed by the change in lattice parameters derived from X-ray diffraction patterns.

5. Conclusions

The coupling of μRaman spectroscopy and μXRD is a major advance in terms of beamline instrumentation. Whereas the coupling of macroscopic probes is often for convenience, combinatorial experiments with microfocus beams demand an *in situ* approach. At micrometre length-scales it is difficult to scan the same region in sequential experiments whilst dynamic studies appear locally unique. Thus, combining these two microfocus techniques together *in situ* opens up many new avenues of research. It is worth pointing out that similar advantages are not enjoyed by combinatorial approaches using macroscopic beams. Large beam sizes serve to average out point-to-point variations making even relatively heterogeneous samples appear as homogeneous. Averaging also makes it easier to repeat static experiments offline, or duplicate dynamic studies with a high degree of precision. Thus with macroscopic beams, *in situ* experiments are often performed without even measuring the same region of the sample (McGeehan *et al.*, 2007; Beale *et al.*, 2005).

Whilst the major advantage of coupling μRaman spectroscopy and μXRD *in situ* remains their temporal and spatial correlation, other minor advantages are also realised. For example, by collecting different data sets together, less time is needed to perform experiments. Less sample material is also required which makes it particularly appropriate for rare or valuable specimens.

The development of the ID13 μRaman system is part of a more general drive towards the use of complementary *in situ* techniques. For example, ID13 has demonstrated simultaneous microfluorescence experiments (Janssens, 2000). Combined WAXS/SAXS/μRaman/microfluorescence is also feasible. As well as sample characterization, such systems may eventually prove useful as sample alignment tools. As beam sizes drop below 200 nm (as envisaged in EH3), optical visualization of the sample is precluded. This will require the development of new ways to manipulate and visualize samples on beamlines. For the continuation of *in situ* Raman spectroscopy, this will certainly require the use of near-field optics which offers spot sizes down to 50 nm (Stöckle *et al.*, 2000).

The authors acknowledge technical assistance from the ID13 beamline support staff, Mr L. Lardiere, Mr M. Perez and Mr H. Gonzalez. Financial support for the microRaman spectrometer is through the EEC FP6 grant (SAXIER).

References

Beale, A. M., van der Eerden, M. J., Kervinen, K., Newton, M. A. & Weckhuysen, B. M. (2005). *Chem. Commun.* **24**, 3015–3017.
Boccaleri, E., Carniato, F., Croce, G., Viterbo, D., van Beek, W., Emerich, H. & Milanesio, M. (2007). *J. Appl. Cryst.* **40**, 684–693.
Bras, W. & Ryan, A. J. (1996). *J. Mol. Struct.* **383**, 309–314.
Bryant, G. K., Gleeson, H. F., Ryan, A. J., Fairclough, J. P. A., Bogg, D., Goossens, J. G. P. & Bras, W. (1998). *Rev. Sci. Instrum.* **69**, 2114–2117.
Chavanne, J., Elleaume, P. & VanVaerenbergh, P. (2000). *ESRF Newsl.* **34**, 29–31.
Cojoc, D., Ferrari, E., Garbin, V., Fabrizio, E. D., Amenitsch, H., Rappolt, M., Sartori, B., Laggner, P., Burghammer, M. & Riekel, C. (2007). *Appl. Phys. Lett.* **91**, 234107.
Davies, R. J., Burghammer, M. & Riekel, C. (2003). *Macromolecules*, **39**, 4834–4840.
Davies, R. J., Burghammer, M. & Riekel, C. (2005). *Appl. Phys. Lett.* **87**, 264105.
Davies, R. J., Burghammer, M. & Riekel, C. (2008). *Macromolecules*, **41**, 7251–7253.
Davies, R. J., Montes-Moran, M. A., Riekel, C. & Young, R. J. (2001). *J. Mater. Sci.* **36**, 3079–3087.
Glisovic, A., Vehoff, T., Davies, R. J. & Salditt, T. (2008). *Macromolecules*, **41**, 390–398.

Hignette, O., Cloetens, P., Lee, W. K., Ludwig, W. & Rostaign, G. (2003). *J. Phys. IV*, **104**, 231– 234.
Janssens, K. (2000). *Microscopic X-ray Fluorescence Analysis*, edited by K. H. A. Janssens, F. C. V. Adams and A. Rindby, p. 211. Chichester: John Wiley and Sons.
Lengeler, B., Schroer, C. G., Benner, B., Guenzler, T. F., Tuemmler, M., Tuemmler, J., Simionovici, A. S., Drakopoulos, M., Snigireva, A. & Snigireva, I. (2001). *Nucl. Instrum. Methods Phys. Res. A*, **467–468**, 944–950.
Lu, S., Russell, A. E. & Hendra, P. J. (1998). *J. Mater. Sci.* **33**, 4721–4725.
McGeehan, J. E., Carpentier, P., Royant, A., Bourgeois, D. & Ravelli, R. B. G. (2007). *J. Synchrotron Rad.* **14**, 99–108.
Martel, A., Burghammer, M., Davies, R. J., DiCola, E., Panine, P., Salmon, J. B. & Riekel, C. (2008). *Biomicrofluidics*, **2**, 02410.
Martel, A., Burghammer, M., Davies, R. J. & Riekel, C. (2007). *Biomacromolecules*, **8**, 3548–3556.
Nöhammer, B. (2004). PhD thesis, University of Neuchâtel, Switzerland.
Nöhammer, B., David, C., Burghammer, M. & Riekel, C. (2005). *Appl. Phys. Lett.* **86**, 163104.
Ran, S., Fang, D., Sics, I., Toki, S., Hsiao, B. S. & Chu, B. (2003). *Rev. Sci. Instrum.* **74**, 3087–3092.
Riekel, C. (2000). *Rep. Prog. Phys.* **63**, 233–262.
Riekel, C. & Davies, R. J. (2005). *Curr. Opin. Colloid Interface Sci.* **9**, 396.
Rodriguez-Cabello, J. C., Martin-Monge, J., Lagaron, J. M. & Pastor, J. M. (1998). *Macromol. Chem. Phys.* **199**, 2767–2776.
Schoeck, J., Davies, R. J., Martel, A. & Riekel, C. (2007). *Biomacromolecules*, **8**, 602–610.
Schroer, C. G., Kurapova, O., Patommel, J., Boye, P., Feldkamp, J., Lengeler, B., Burghammer, M., Riekel, C., Vincze, L., van der Hart, A. & Küchler, M. (2005). *Appl. Phys. Lett.* **87**, 124103.
Stöckle, R. M., Suh, Y. D., Deckert, V. & Zenobi, R. (2000). *Chem. Phys. Lett.* **318**, 131.
Torre, J., Cortázar, M., Gómez, M. A., Marco, C., Ellis, G., Riekel, C. & Dumas, P. (2006). *Macromolecules*, **39**, 5564–5568.